Error Analysis of Doppler velocity retrievals using a spaceborne cloud radar DPCA system

V. Venkatesh*, S. Tanelli*, S. Durden*, R. Beauchamp*

* Jet Propulsion Laboratory, California Institute of Technology

*

July 6, 2021

Abstract

Spaceborne measurements of Doppler velocity, although capable of adding valuable insights on latent heating and cloud microphysics, remain undemonstrated through NASA's storied history. The challenge has been that the projection of spacecraft speeds within the antenna beam results in large spectral width. Since the Doppler spectrum and the auto-correlation function form a Fourier pair, broad Doppler spectra leads to rapid decorrelation and high estimation errors in the Doppler velocity.

Previous work by Durden and Tanelli have suggested the use of the Displaced Phase Center Antenna (DPCA) technique for Doppler measurements of distributed scatterers from spaceborne platforms. The proposed technique aims to compensate/freeze the antenna pattern such that there is little relative motion between the platform and the scatterers. This work develops a holistic framework to assess estimation errors in Doppler velocities with the DPCA technique. As a secondary goal, propagated errors in subsequent full wind-field retrievals are also investigated.

Index Terms

Signal processing, Monte-Carlo simulation, Millimeter wave radar.

*Corresponding author email : vijay.venkatesh@jpl.nasa.gov .

I. THEORETICAL FORMULATION

Displaced Phase Center Antenna (DPCA) systems comprise of two antennas displaced in the along-track dimension [1] [2]. As the spacecraft flies along, the basic idea is to sequentially sample nearly the same location on the cloud at offset instances in time. The relative phase change between the measurements at the two antennas is then scaled to estimate Doppler velocity of the cloud particles.

In order to investigate the performance of a DPCA system, consider a nadir looking multi-antenna radar system pointed at a collection of Rayleigh scatterers. Let the antenna phase centers be located at $(-\frac{\Delta x}{2}, 0, -r_0)$ and $(\frac{\Delta x}{2}, 0, -r_0)$. In the geometry in Fig. 1, we define origin to be at the range bin of interest, and centered between the DPCA antennas. Let "1" and "2" denote the aft and fore antennas at times t and $t+\tau$ respectively. Denote the correlation coefficient between the received voltages at the fore and aft antennas as $\gamma(\Delta x, \tau)$.

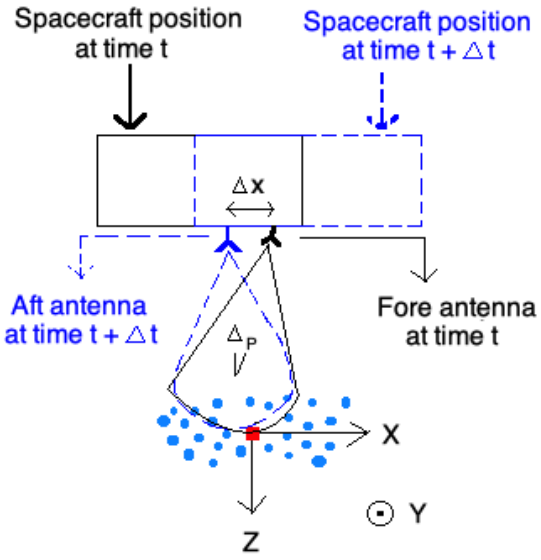

Fig. 1: Illustration of the co-ordinate system used in the theoretical formulation herein. Origin (indicated by the red rectangle) is located at the center of the resolution volume. For convenience, the radar is assumed to probe the resolution volume at nadir. Symbols used in modeling the correlation between two complex voltages at the fore/aft antenna pair are indicated in table 1.

Following [3], the received voltages at TR_1 and TR_2 due to a collection of randomly located

TABLE I: Symbols used in modelling correlation between received voltages at the fore and aft antennas of a spaceborne DPCA system.

Symbol	Meaning	Units
k	Wavenumber corresponding to radar frequency	m^{-1}
C	Radar constant	Vm^{-2}
Δx	Along-track distance between fore/aft antenna pair	m
τ	Lag used to synthesize DPCA system	m
σ_{RCS}	Radar cross section of single scatterer	m^2
n	Number density of scatterers	m^2
g_1	Effective two-way antenna gain for aft antenna	
g_2	Effective two-way antenna gain for fore antenna	
r_0	Range to resolution volume	m
$x^{''}$	x-cordinate of scatterer location	m
$y^{''}$	y-cordinate of scatterer location	m
$z^{''}$	z-cordinate of scatterer location	m
$r^{''}$	Scatterer location as a function of $x^{''}$, y and $z^{''}$	m
$\sigma_{e\phi}$	Second central moment of two-way azimuth pattern	rad
σ_{θ}	Second central moment of two-way elevation pattern	rad
σ_R	Range resolution	m
v_x	Baseline velocity (wind-component along $x^{''}$)	ms^{-1}
v_y	Cross-baseline velocity (wind-component along $y^{''}$)	ms^{-1}
v_z	Radial velocity (wind-component along $z^{''}$)	ms^{-1}
σ_{tz}	RMS turbulent velocity along $z^{''}$	ms^{-1}
M	Number of independent samples within dwell	unitless

Rayleigh scatterers is given by

$$V_1^*(t) = C \int_{V''} n\sigma_{RCS} A_1(r'') W(r'') \exp\{2jk(|r''\vec{}_{TR_1}(t)|dV'', \tag{1}$$

$$V_2(t+\tau) = C \int_{V''} n\sigma_{RCS} A_2(r'') W(r''). \exp\{-2jk(|r''\vec{}_{TR_2}(t)|dV'' \tag{2}$$

where $|\vec{r''}_{TR_1}|$ denotes the distance from the aft antenna phase-center to the scatterer, $|\vec{r''}_{TR_2}|$ denotes the distance from the fore antenna phase-center to the scatterer. As the scatterers advect, these distances change as a function of time. In equations (1) and (2), C denotes an instrument dependent constant, k denotes the radar wavenumber, σ_{RCS} denotes the scattering cross-section and n denotes the number density of the scatterers. By omitting the dependence of σ_{RCS} and n on r'', we have implicitly assumed homogeneity of scattering cross-sections in the resolution volume. A_1 and A_2 are the effective antenna weighting functions of the fore and aft apertures respectively and are given by

$$A_1(r'') = g_1 \exp\{-\frac{(x''(t) - x_1)^2}{2r_0^2\sigma_{\phi R_1}^2} - \frac{y''^2(t)}{2r_0^2\sigma_\theta^2}\} \tag{3}$$

$$A_2(r'') = g_2 \exp\{-\frac{(x''(t) - x_2)^2}{2r_0^2\sigma_{\phi R_2}^2} - \frac{y''^2(t)}{2r_0^2\sigma_\theta^2}\} \tag{4}$$

where x_1 and x_2 are the x-coordinates of TR_1 and TR_2 respectively. Here $\sigma_{\phi TR_1}$ and $\sigma_{\phi TR_2}$ are the second central moments of the antenna patterns in the azimuthal plane. The effect of pulse width on volumetric scattering is captured by the range weighting function, and is given by

$$W(r'') = \exp\{-\frac{z''^2(t)}{4\sigma_R^2}\}. \tag{5}$$

Following [4], a second order Taylor series expansion of the phase-terms of $V_1^*(t)$ and $V_2^*(t+\tau)$ around origin gives

$$|\vec{r''_{TR_1}}| = r_0 + z''(t) + \frac{(x''(t) - x_1)^2 + y''^2(t)}{2r_0}, \tag{6}$$

$$|\vec{r''_{TR_2}}| = r_0 + z''(t) + \frac{(x''(t) - x_2 - r_0 \sin\Delta_p)^2 + y''^2(t)}{2r_0}, \tag{7}$$

where $|r_0\vec{TR_1}| \simeq |r_0\vec{TR_2}| \simeq r_0$. In the rest of this section, we omit the notation "(t)" for scatterer positions. It is implicit that x'', y'' and z'' are time dependent. Note that the range to the coordinate system origin r_0 is time-invariant. Substituting (6) and (7) in (1), we get

$$V_1^*(t) = C\ n\ \sigma_{RCS}\ \exp\{2jkr_0\}\ I_{x_1} I_{y_1} I_{z_1} \tag{8}$$

where,

$$I_{x_1} = \int_{x''} exp\{-\frac{(x'' - x_1)^2}{2r_0^2\sigma_\phi^2}\} exp\{j\frac{x''^2 + (x'' - x_1)^2}{2r_0}\} dx'', \tag{9}$$

$$I_{y_1} = \int_{y''} exp\{-\frac{y^{2''}}{2r_0^2\sigma_\theta^2}\} exp\{j\frac{y''^2}{r_0}\} dy'', \tag{10}$$

$$I_{z_1} = \int_{z''} exp\{-\frac{z^{2''}}{4\sigma_R^2}\} exp\{2jkz''\} dz''. \tag{11}$$

In equation (9), the "$x'' - x_1$" terms correspond to weighting by the aft receive beam. To evaluate $V_2(t+\tau)$, we set $\vec{r}(t+\tau) = \vec{r}(t) + \vec{v}(t)\tau$. In the rest of this section, we omit the time dependence of $\vec{v}$ on t. Substituting these relationships in (2), we get

$$V_2(t+\tau) = C\ n\ \sigma_{RCS}\ \exp\{-2jkr_0\}\ I_{x_2} I_{y_2} I_{z_2} \tag{12}$$

where,

$$I_{x_2} = \int_{x''} exp\{-\frac{(x'' - x_2 + v_x\tau)^2}{2r_0^2\sigma_\phi^2}\} exp\{j\frac{(x'' + v_x\tau)^2 + (x'' - x_2 - r_0 \sin\Delta_p + v_x\tau)^2.}{2r_0}\} dx'', \tag{13}$$

$$I_{y_2} = \int_{y''} exp\{-\frac{(y'' + v_y\tau)^2}{2r_0^2\sigma_\theta^2}\} exp\{j\frac{(y'' + v_y\tau)^2}{r_0}\} dy'', \tag{14}$$

$$I_{z_2} = \int_{z''} exp\{-\frac{(z'' + v_{nz}\tau)^2}{4\sigma_R^2}\} exp\{2jk(z'' + v_{sum,z}\tau)\} dz''. \tag{15}$$

where v_x is the mean translational wind-component along x'' and v_y is the mean translational wind-component along y''. The covariance between the received voltages at the fore and aft antennas at lag τ can be written as

$$c_{12}(\Delta x, \tau) = (Cn\sigma_{RCS})^2 \langle I_{x_1} I_{x_2}\rangle \langle I_{y_1} I_{y_2}\rangle \langle I_{z_1} I_{z_2}\rangle. \tag{16}$$

The integrals evaluate to

$$I_{x_1} I_{x_2} = \sqrt{\pi}\sigma_{e\phi} r_0 \exp\{-2k^2\sigma_{e\phi}^2 (v_x\tau - \Delta x)^2\}, \tag{17}$$

$$I_{y_1} I_{y_2} = \sqrt{\pi}\sigma_\theta r_0 \exp\{-2k^2\sigma_\theta^2 v_y^2 \tau^2\}, \tag{18}$$

$$I_{z_1} I_{z_2} = \sqrt{2\pi}\sigma_R \exp\{-2jkv_{sum,z}\tau\}. \tag{19}$$

Here, Δx is the effective distance between the phase centers of equivalent monostatic TR_1 and TR_2 combinations. This is the projection of the vector joining the two resolution volume centers onto the unit vector $\widehat{x}$ and is given by

$$\Delta x = \vec{r}_{TR_1TR_2} \cdot \widehat{x} = r_0 \sin(\Delta_p) + x_2 - x_1. \tag{20}$$

where $\widehat{x}$ is the unit vector along the x-axis,, Δx is the physical distance between the phase-centers of the fore and aft apertures, x_1 and x_2 are the x-cordinates of the fore and antenna phase centers. To proceed, we approximate the expectations of $I_{x_1} I_{x_2}$ and $I_{y_1} I_{y_2}$ by themselves. This is tantamount to neglecting fluctuations of v_x and v_y. The reasoning is that the $z^{''}$-component of velocity turbulence causes the most phase fluctuations and overwhelms sensitivity to $x^{''}$- and $y^{''}$-components of fluctuations. Therefore, it suffices to evaluate the ensemble average of the $z^{''}$-component of velocity turbulence alone. To evaluate the expectation of $I_{z_1} I_{z_2}$, we decompose $v_{sum,z}$ into its mean and turbulent components.

$$\langle I_{z_1} I_{z_2} \rangle = \langle \sqrt{2\pi}\sigma_R \exp\{-2jk(v_{mz} + v_{tz})\tau\} \rangle \tag{21}$$

$$\langle I_{z_1} I_{z_2} \rangle = \sqrt{2\pi}\sigma_R \exp\{-2jkv_{mz}\tau\} \int_{-\infty}^{\infty} \exp\{-2jkv_{tz}\tau\} p(v_{tz}) dv_{tz}. \tag{22}$$

Here, $p(v_{tz})$ is the probability density function of the $z^{''}$-component of velocity turbulence. The specific form of (22) depends on the probability density function (PDF). Using (17), (18) and (22) in (16) and normalizing, we arrive at a general form for the correlation function

$$\gamma(\Delta x, \tau) = \exp\{-2k^2\sigma_{e\phi}^2 (v_x\tau - \Delta x)^2\} \exp\{-2k^2\sigma_\theta^2 v_y^2 \tau^2\} \gamma_{turb}(\tau) \exp\{-2jkv_{mz}\tau\} \tag{23}$$

where,

$$\gamma_{turb}(\tau) = \int_{-\infty}^{\infty} \exp\{-2jkv_{tz}\tau\} p(v_{tz}) dv_{tz}. \tag{24}$$

where $p(v_{tz})$ is the probability density function of velocity turbulence. The specific form of (24) depends on the probability density function (PDF). The conditions in which the PDF $p(v_{tz})$ can be approximated as Gaussian is an ongoing debate [5] [6] [7] First, there is a dependence on the sensitivity of the observing geometry to the spatial spread in hydrometeor fall velocity within the resolution volume. Second, it also depends on the largest dimension of the resolution volume relative to the scale at which velocity turbulence is introduced (i.e. the outer scale). Notwithstanding these conditions, the assumption of Gaussian wind-field statistics is commonplace in the cloud radar community. Assuming that $p(v_{tz})$ is Gaussian, we proceed as

$$\langle I_{z_1} I_{z_2} \rangle = \sqrt{2\pi}\sigma_R \exp\{-2jkv_{mz}\} \int_{-\infty}^{\infty} \exp\{-2jkv_{tz}\} \frac{exp\{-\frac{v_{tz}^2}{2\sigma_{tz}^2}\}}{\sqrt{2\pi\sigma_{tz}}} dv_{tz} \tag{25}$$

$$\langle I_{z_1} I_{z_2} \rangle = \sqrt{2\pi}\sigma_R \exp\{-2jkv_{mz}\} exp\{-2k^2\sigma_{tz}^2\tau^2\} \tag{26}$$

Normalizing by the auto-covariance at zero-lag, we get

$$\langle \gamma(\Delta x, \tau) \rangle = \exp\{-2k^2\sigma_{e\phi}^2(v_x\tau - \Delta x)^2\} \exp\{-2k^2\sigma_\theta^2 v_y^2\tau^2\} exp\{-2k^2\sigma_{tz}^2\tau^2\} \exp\{-2jkv_{mz}\tau\} \tag{27}$$

To estimate Doppler velocity, an inversion of the forward model in equation (27) yields

$$\langle \widehat{v}_{mz} \rangle = -\frac{1}{2k\tau} \angle \langle \widehat{\gamma}(\Delta x, \tau) \rangle. \tag{28}$$

Following [4], the variance of $\widehat{v}_{mz}$ can be accessed as a function of the correlation model in equation (27) using the relationship

$$var[\widehat{v}_{mz}(\Delta x, \tau)] = \frac{\lambda^2}{32\pi^2\tau^2} \frac{(1 + SNR)^2 - |\gamma(\Delta x, \tau)|^2}{M|\gamma(\Delta x, \tau)|^2}. \tag{29}$$

II. Monte-Carlo simulation results

To benchmark the performance of DPCA systems across the design space, a Monte-Carlo simulator was developed. Results in this section showcase the performance over the design space, while also validating the theoretical results in the previous section.

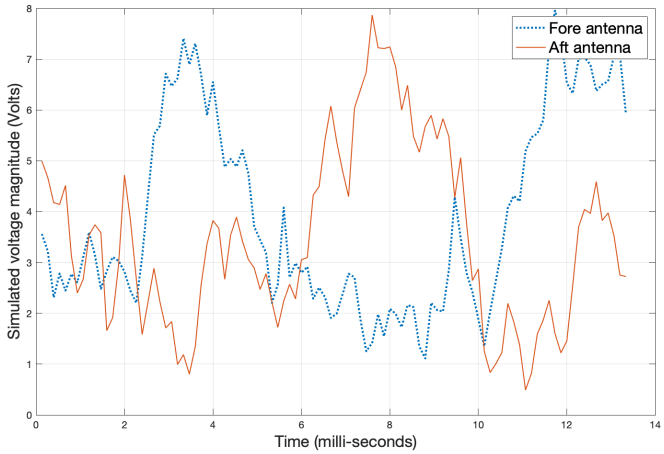

Fig. 2: Monte-Carlo simulation of received voltages at the fore and aft antennas. As expected, voltages recevied at the aft antenna lag voltages at the fore antenna. The voltages are otherwise similar.

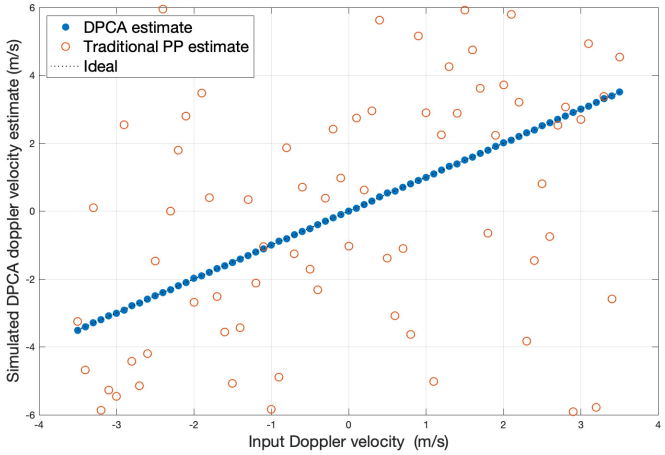

Fig. 3: Comparison of DPCA Doppler velocity retrievals with traditional pulse-pair retrievals for an antenna size of 1 m. The outperformance of the DPCA system is apparent.

To understand the design space of DPCA spaceborne cloud radars, emphasis has been placed on the following degrees of freedom :

1) Baseline
2) Pulse repetition time
3) Antenna size
4) Antenna orientation for subsequent wind-field retrievals using dual-Doppler techniques.

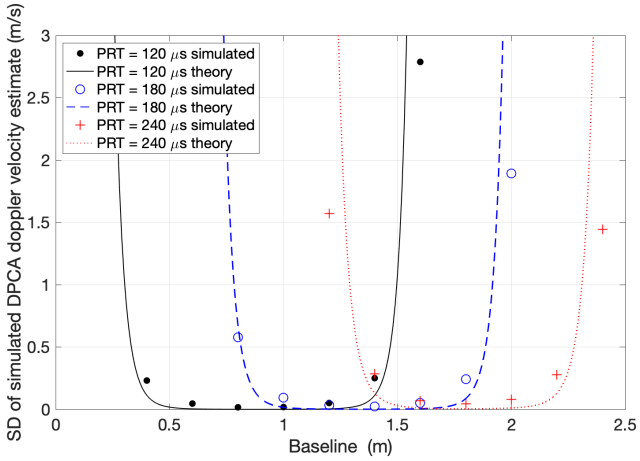

Fig. 4: Validation of theoretical results with Monte-Carlo simulations. An RMS velocity turbulence of 3 m/s was used to benchmark simulation results in this section.

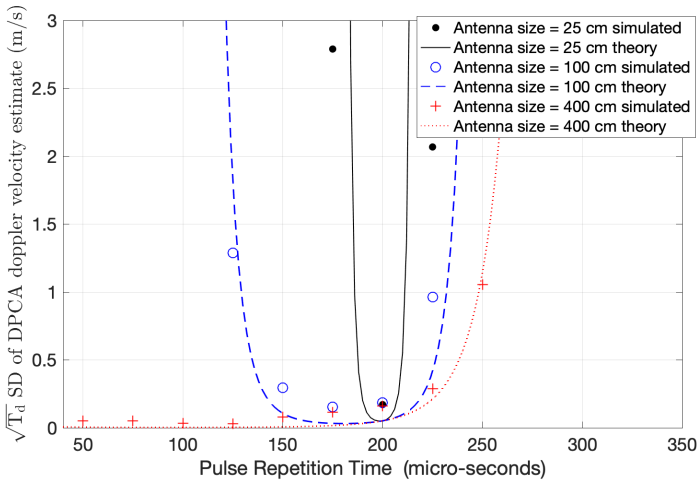

Fig. 5: Both theory and simulations show that DPCA systems with precisely chosen pulse repetition times enable designs with antenna sizes as small as 25 cm.

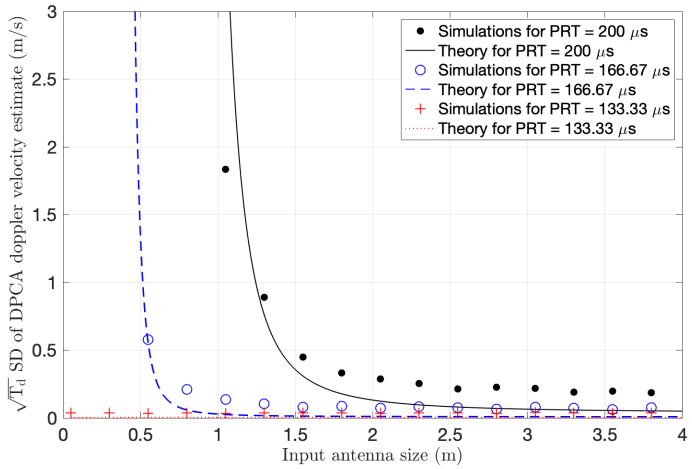

Fig. 6: Both theory and simulations show that antenna size of 75 cm is sufficient to enable a range of pulse repetition times for instrument operation. This enables velocity unfolding and subsequent wind-field retrievals.

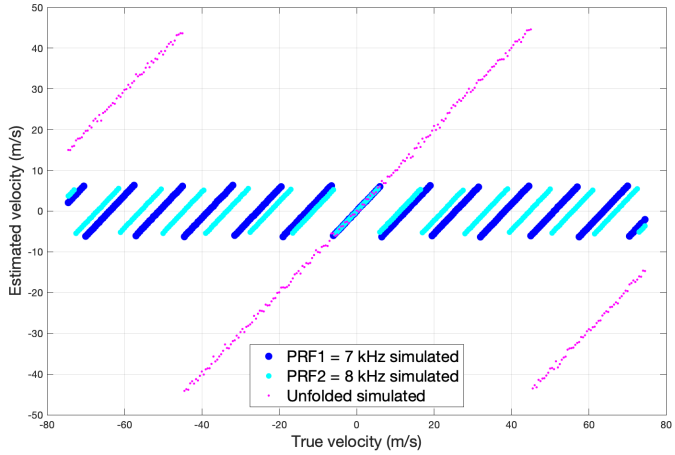

Fig. 7: Monte-Carlo simulations showing unfolded Doppler velocities for a 7:8 pulse repetition time ratio. Sufficient fidelity of unfolded Doppler velocites led to a subsequent investigation of wind-field retrievals.

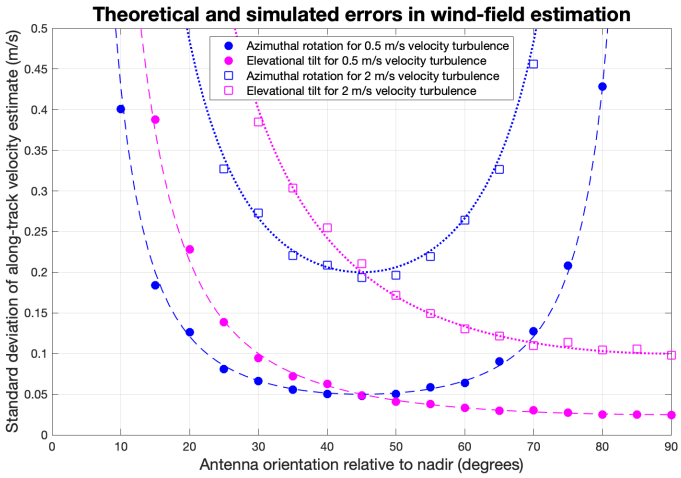

Fig. 8: Comparison of theoretical predictions with simulation results for DPCA along track wind component retrievals. Both theory and simulations suggest off-nadir tilts of around 45 degrees.

REFERENCES

[1] S. Durden, S. Tanelli, and P. Siqueira, "On the use of multi-antenna radars for spaceborne doppler precipitation measurements," vol. 4, pp. 181–183, 2007.

[2] S. Tanelli, S. Durden, and M. Johnson, "Airborne demonstration of dpca velocity measurements for distributed targets," vol. 13, pp. 1415–1419, 2016.

[3] R. J. Doviak, R. J. Lataitis, and C. L. Holloway, "Cross correlations and cross spectra for spaced antenna wind profilers part i: Theoretical analysis," *Radio Sci.*, vol. 31, pp. 157–180, 1996.

[4] R. J. Doviak and D. S. Zrnić, *Doppler Radar and Weather Observations, 2nd ed.* Academic Press, 1993.

[5] M. Fang and R. Doviak, "Coupled contributions in the radar spectrum width equation," *J. Atmos. Oceanic. Tech.*, vol. 25.12, pp. 2245–2258, 2008.

[6] T.-Y. Yu, R. Rondinel, and R. Palmer, "Investigation of non-gaussian spectra observed by weather radar in a tornadic supercell," *J. Atmos. Oceanic. Tech.*, vol. 26, pp. 444–452, 2009.

[7] M. Fang, R. Doviak, and B. Albrecht, "Analytical expressions for doppler spectra of scatter from hydrometeors observed with a vertically directed radar beam," *J. Atmos. Oceanic. Tech.*, vol. 29.4, pp. 500–509, 2012.